AUT Journal of Electrical Engineering
10.22060/EEJ.2026.25018.5819

An Innovative Falcon Optimized PI Controller With ANN Controller for Dual PV Powered EV Charging System

Bollu Prabhakar[1*], Golla Satyanarayana[2], Gummala H V S Prasad[3], Kaki Kasi Venkata Prakash[4], Manne Vinisha Sai[5]

[1,2]Assistant Professor, Department of Electrical & Electronics Engineering, Godavari Institute of Engineering and Technology (A), Rajahmundry, India.
[3,4,5]UG Scholar, Department of Electrical & Electronics Engineering, Godavari Institute of Engineering and Technology (A), Rajahmundry, India.
*Corresponding author Email: bolluprabhakar237@gmail.com

Abstract:

Electric Vehicles (EV's) are measured as an excellent replacement for fuel based vehicle due to their limited emission of greenhouse gases. Despite that, it is essential to establish better EV charging system to enlarge EV utilization. Thus, this paper proposes an enhanced EV charging process based on dual PhotoVoltaic (PV) using High Gain Luo converter with optimized PI controller. High Gain Luo Converter is deployed for both PV system for boosting their output power supply, which enables to achieve higher efficiency with improved Voltage gain, power quality with reduced ripples. For attaining enhanced converter performance, Falcon Optimized Algorithm (FAO) based PI controller is utilized which enables faster response rate with reduced steady-state errors with higher quality results. Furthermore, Bidirectional DC-DC (BDC) converter is utilized to attain overall charging and discharging level of EV battery where separate ANN controllers are employed for monitoring and controlling the charging operation as well as bidirectional converter. Moreover, to determine performance proficiency of proposed system, MATLAB simulation is implemented, from which it is remarkable that dual PV powered EV charging system attained higher efficiency of (95.73%), Voltage gain and reduced THD of (2.87). Therefore, this system ensures superior EV charging with continuous power supply and accurate detection of EV charging level.

Keywords:

EV, PV system, High Gain Luo Converter, FOA based PI controller, Bidirectional DC-DC converter, ANN controller, VSI and EV charging system.

AUT Journal of Electrical Engineering
10.22060/EEJ.2026.25018.5819

1. Introduction

The growing public alertness towards environmental pollution and fossil fuel reduction leaded to drastic demand of EV, an alternative for Internal Combustion Engine (ICE). However, EV charging still faces certain difficulties like longer charging time and insufficient charging points hence, for the development of sustainable and unlimited energy supply, PV power is utilized [1,2]. PV is the vital source for charging to produce clean and reliable energy with minimized implementation cost [3]. Moreover, integration of PV in charging system enables to obtain reduced power losses with minimized pressure on charging system thereby, increasing reliability of EV charging process [4,5]. Furthermore, to enhance the low output power obtained from PV, converter is an essential need, DC-DC converter is introduced to PV source for attaining increased power output throughout varying operating conditions [6]. Comparatively, Boost, Cuk [7] and Buck converters enables to attain enhanced voltage conversion with fast charging capacity and reduced power losses [8]. However, these converters produce unstable current and voltage supply with increased noise, poor efficiency and high ripples. The Luo converter [9] offers high voltage gain, lower output ripple, and enhanced power transfer efficiency, which makes it an effective choice for PV-based EV charging systems. Nevertheless, traditional Luo converters experience switching losses and increased voltage stress during dynamic operating conditions, motivating the need for the proposed modified High Gain Luo converter.

Despite this, to regulate and stabilize the output, controller play a vital role hence, PI controller is considered as they enable simple and easy implementation with minimized steady-state errors but PI controllers struggle with certain drawbacks such as overshoot, instability and fluctuation therefore to reduce the oscillations and errors associated with PI controller, parameter tuning is obligated [10]. Henceforth, Lion Grey Wolf Optimized Proportional Integral (LGWO) based PI controller is implemented, which improves

10.22060/EEJ.2026.25018.5819

output voltage obtained from converter along with reduced settling time inducing better system reliability and efficiency [12]. Nevertheless, this LGWO controllers struggles with low convergence rate with inaccuracy. Similarly, traditional optimization techniques like P&O, Genetic Algorithm Optimization (GAO) [12] and Salp Swarm Algorithm (SSA) are considered for enabling enhanced parameter tuning with reduced fluctuations and interferences but these techniques do not provide desired tuning performance due to their longer tuning time and instability [13]. Thus, the proposed work utilizes Falcon Optimised PI controller for overcoming the conventional approaches by producing stabilized output with reduced settling time and rapid convergence speed. The contributions of developed sustainable PV based EV charging system are discussed below,

- Dual PV system is deployed for enabling sufficient and enhanced EV charging system
- The integration of High Gain Luo converter delivers high voltage gain with larger output and reduced ripple generating high level output voltage
- The implementation of Falcon Optimised PI controllers ensures stable and regulated output voltage thereby, enabling higher efficient charging system.
- Incorporating bidirectional converter with ANN controller for providing bidirectional power flow and to regulate the converter with efficient monitoring of battery.

2. Proposed Modelling

To obtain sustainable and efficiecnt EV charging system, PV system is considred as a primary source due to its clean and unlimited power supply however, due to varying weather conditions, obtaining enhnaced power output from PV remians challenging. Thus, to progress PV allocated EV charging system utilizing High Gain Luo converter with FOA-PI controller for providing highly effectual, stable and sustainable output as displays in Figure 1.

AUT Journal of Electrical Engineering
10.22060/EEJ.2026.25018.5819

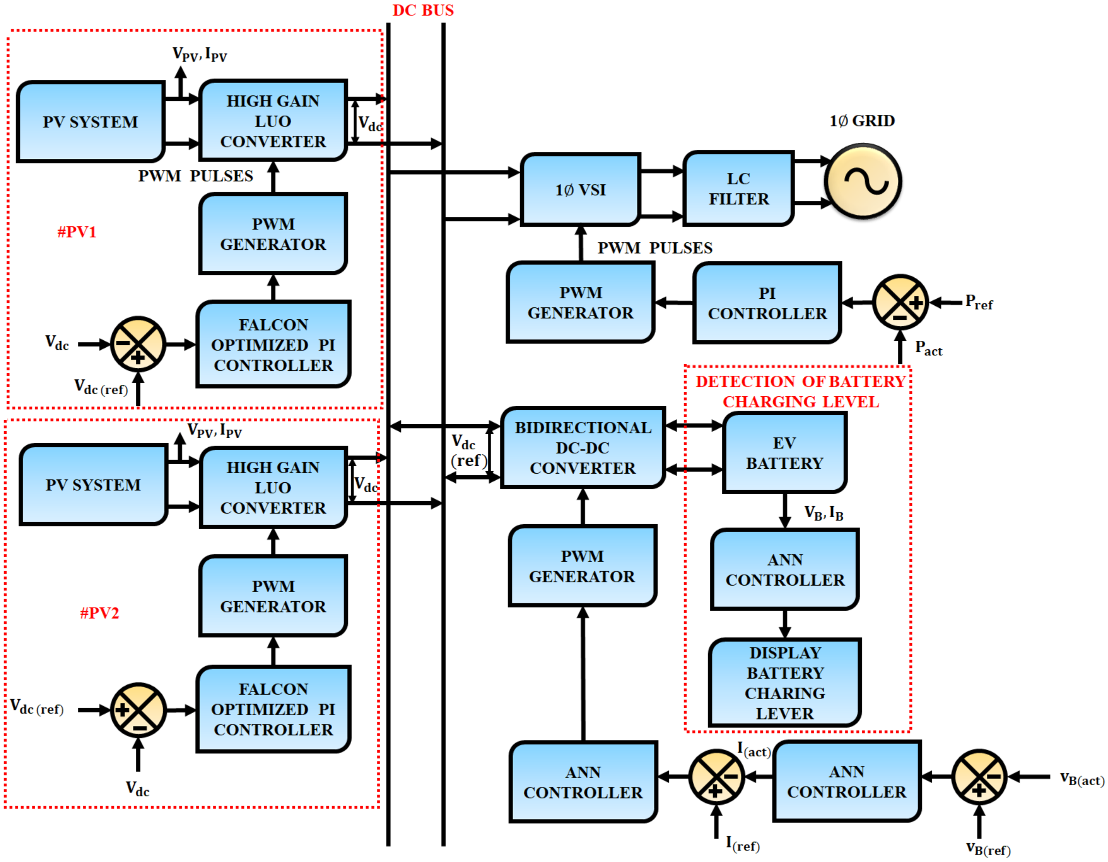

Fig. 1. PV based EV charging System

Initailly, PV absorbs the energy from sunlight and solar radiation to produce power output but the power obtained from PV contains low voltage level hence, to boost the output power to high voltage level, High Gain Luo converter is deployed which generates desired output level with higher efficiency. Additionally, to regulate and stabilize the output, PI controllers is implemented for which, parameter tuning is attained by Falcon Optimization technique. Furthermore, the output from PV structure is tranferred to EV battery through DC-bus and for preserving charging and discharging level of EV battery, Bi-directional DC-DC converter is utilised. Besides, the converter is efficiently structured via ANN controller. Other ANN controller is deployed on the EV battery side for monitoring the battery state to provide accurate and precise detection of battery charging level. Finally, surplus power produced from PV is fed to the grid system.

Therefore, the developed system as a whole ensures to attain better performance in terms of fast, stable and sustainable EV charging with high durability.

2-1- PV System

In this system, the solar module is utilised for generating power supply by absorbing the sunlight. Solar PV cells consisting of a Single Diode is depicted in Figure 2 where I_{Ph} and I_s reprsents PV current and reverse saturation current whereas, V reprsents output voltage of PV cell connected in series and V_T represents thermal voltage. Therefore,

$$V_T = k * T * \frac{a}{q} \tag{1}$$

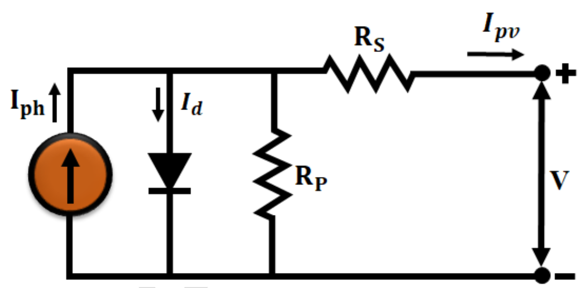

Fig. 2. Solar PV cell

Where, ‘k’ is the Boltzmann constant, ‘T’ denotes p-n junction temperature and ‘a’ denotes ideality constant of diode and ‘q’ is charge of electron. Hence, output current from PV cell is stated using,

$$I = I_{Ph} - I_S \left[exp\left(\frac{V + IR_S}{nV_T} \right) - 1 \right] \tag{2}$$

Output of PV module is low owing to its unstable circumstances, thus to boost it into maximize level, the suggested work develop High gain Luo converter as discussed below.

2-2- Modelling of High Gain Luo Converter

10.22060/EEJ.2026.25018.5819

Implementation of High Gain Luo converter generates enlarged power output with better system proficiency. This converter produces output with reduced ripple and high-power density with minimized cost of installation which is accomplished by utilizing inductor and capacitor in power circuits. Figure 3 represents circuit diagram of High Gain Luo converter which consists of single switch S, Diodes D_1 and D_2, capacitor C_0 and $C_1$and inductors L_1 and L_2 respectively. Luo converter function based on two modes.

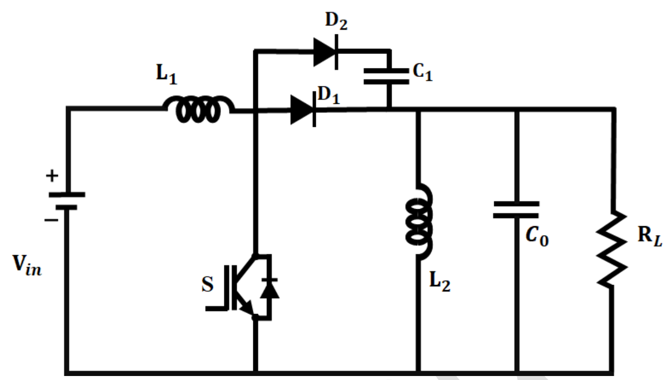

Fig. 3. Circuit diagram of High Gain Luo converter

Mode 1: In mode 1, switch S remains ON with diode D_1 ON while D_2 is turned OFF. Therefore, inductors L_1 and L_2 store and the energy is discharged through C_0 and supplied to R_L as depicted in Figure 4.

$$V_{in} - V_{L1} = 0,\ V_{in} = V_{L1} \tag{3}$$

$$V_{C1} - V_{L2} = 0,\ V_{C1} = V_{L2} \tag{4}$$

$$V_{L2} = V_{C0} = V_0 \tag{5}$$

By, substituting (3) in (2),

$$V_{C1} = V_0 \tag{6}$$

10.22060/EEJ.2026.25018.5819

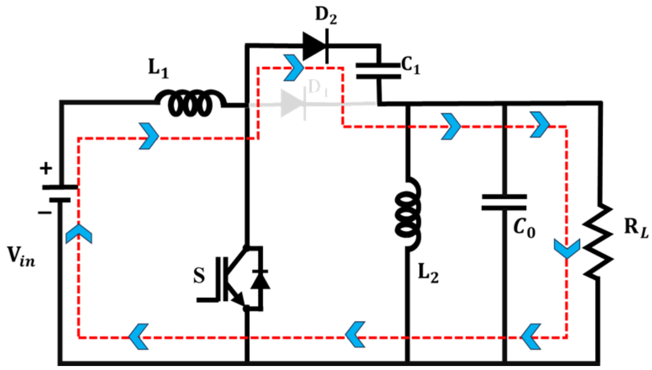

Fig. 4. Converter operation mode 1

Mode 2: In mode 2, Switch S is kept OFF whereas, diodes D_1 is turned ON and D_2 is turned OFF which makes inductors L_1 and L_2 to discharge and supply load R_L while capacitor C_0 store as depicted in Figure 5.

$$V_{in} - V_{L1} - V_{L2} = 0 \tag{7}$$

$$V_{L2} = V_0 \tag{8}$$

By substituting (6) in (5),

$$V_{in} - V_{L1} - V_0 = 0 \tag{9}$$

$$V_{L1} = V_{in} - V_0 \tag{10}$$

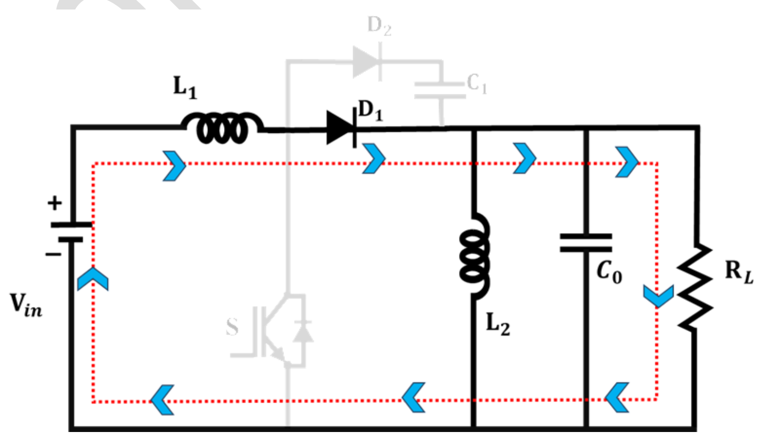

Fig. 5. Converter Operation mode 2

Where V_{L1}, V_{L2} represent the voltage across inductors, V_{C0}, V_{C1} represents the voltage across the capacitors, V_{in} denotes input voltage and V_0 denotes output voltage respectively. Overall converter voltage gain is measured using,

$$\left(V_{L1,\ SW\ close}\right)(DT) + \left(V_{L1,\ SW\ open}\right)(1-D)T = 0 \tag{11}$$

On substituting (1) and (8) in (9) gives,

$$V_{in}(DT) + (V_{in} - V_0)(1-D)T = 0 \tag{12}$$

$$\frac{V_0}{V_{in}} = \frac{(2D+1)}{(1-D)} \tag{13}$$

Where equation (13) indicates the overall voltage gain and Figure 6 represents switching waveform of the developed converter.

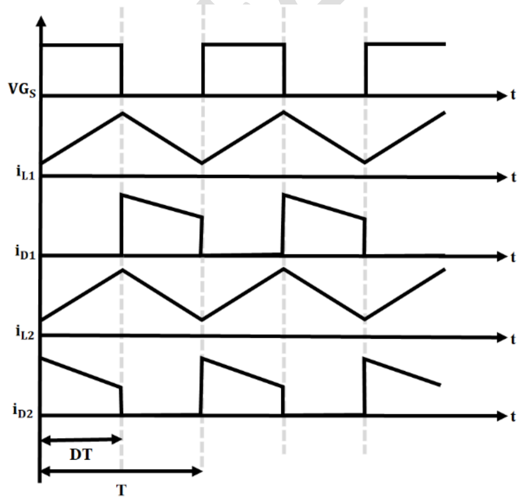

Fig. 6. Switching Waveform High Gain Luo converter

Here, the output energy of PV is highly boosted up into the required level of EV battery to support proposed converter. Also, PI controller is employed for producing stable output and to tune the parameters of PI, the falcon optimization approach is utilized as described as follows.

2-3- Modelling of Falcon Optimized PI Controller

10.22060/EEJ.2026.25018.5819

Under varying irradiance, temperature and load circumstances, the PI controller's goal is to diminish settling time, overshoot and steady-state error while managing the DC-link voltage of the High Gain Luo converter at the reference value. In this work, the FOA minimises the objective function to predict the ideal K_p, K_i, as,

$$J = \int_0^T e^2(t)\,dt \tag{14}$$

$$e(t) = V_{ref} - V_{dc} \tag{15}$$

This goal assures precise voltage control, keeps the output voltage within the specified tolerance (±5%) and permits the converter to reach a maximum efficiency with steady dynamic performance and lower steady-state error.

The Falcon Optimization Algorithm [14] is a meta-heuristic approach that works based on falcons hunting strategy. The hunting manner of falcons varies based on falcons preferences and performs specific hunting strategies for seeking their prey by exhibiting circular and definite paths for attacking their prey. The hunting strategy of falcon is commonly divided into two segments namely, spiral logarithmic and straight forward segments. Spiral logarithmic stage is where falcon looks at the prey through side-eye maintaining straight head whereas, in straight forward segment, falcon ejects at target in straight line and further swoops the target using binocular vision.

Henceforth, the hunting process of falcon is further categorized into prey seeking, spiral logarithmic and straight dive in which initial position of falcon is placed arbitrary in D-dimensional space where 'X' reprsents the position of the falcon and 'NP' represents their quantity in dimensional space D.

$$X = \begin{bmatrix} X_{11} & X_{1,D} \\ X_{NP,1} & X_{NP,D} \end{bmatrix} \tag{16}$$

The initial velocities produced is given by,

10.22060/EEJ.2026.25018.5819

$$V_{Max} = 0.1U_b \tag{17}$$

$$V_{Min} = -V_{Max} \tag{18}$$

Where, V_{Max} and V_{Min} represents maximum and minimum velocities and U_b represents upper bound range limit. Moreover, based on regulations, fitness of each and every falcon is measured and finest one is considered as g_{best} and falcons finest positions is considered as X_{best}, which are taken into account for producing newest position.

At the initial conditions, for comparing Awareness Propability (AP) and Dive Probability (DP), each falcon is assigned with arbitrary Pairing values (pAP, pDP) with equal distribution. Accordingly, if pAP is less than AP, it said that falcon prey seeking and is given by,

$$X(k+1) = X(k) + V(K) - C_C r\left(X_{best}(k) - X(k)\right) + S_c r\left(g_{best}(k) - X(k)\right) \tag{19}$$

Where 'k' represents iteration procedure, when pAP is higher than AP, then DP is compared with pDP and if pDP is higher than DP, then X_{Chosen} prey is selected by falcon. Afterwards, spiral logirthmic segment is exhibit by falcon for hunting which is expressed using,

$$X(k+1) = X(k) + \left|X_{Chosen} - X(k)\right| \exp(bt)\cos(2\pi t) \tag{20}$$

Here 'b' represents spiral logrithmics and 't' is arbitary values between [-1,1]. If pAP is less than AP, then selected prey fitness is compared with falcon fitness which is given by,

$$X(k+1) = X(k) + V(k) + f_c r\left(X_{Chosen} - X(k)\right) \tag{21}$$

(or)

$$X(k+1) = X(k) + V(k) + C_C r\left(X_{best}(k) - X(k)\right) \tag{22}$$

Hence, above process loops until desired conditons are obtained amd the flow chart of the FAO based PI controller is depicted in Figure 7.

10.22060/EEJ.2026.25018.5819

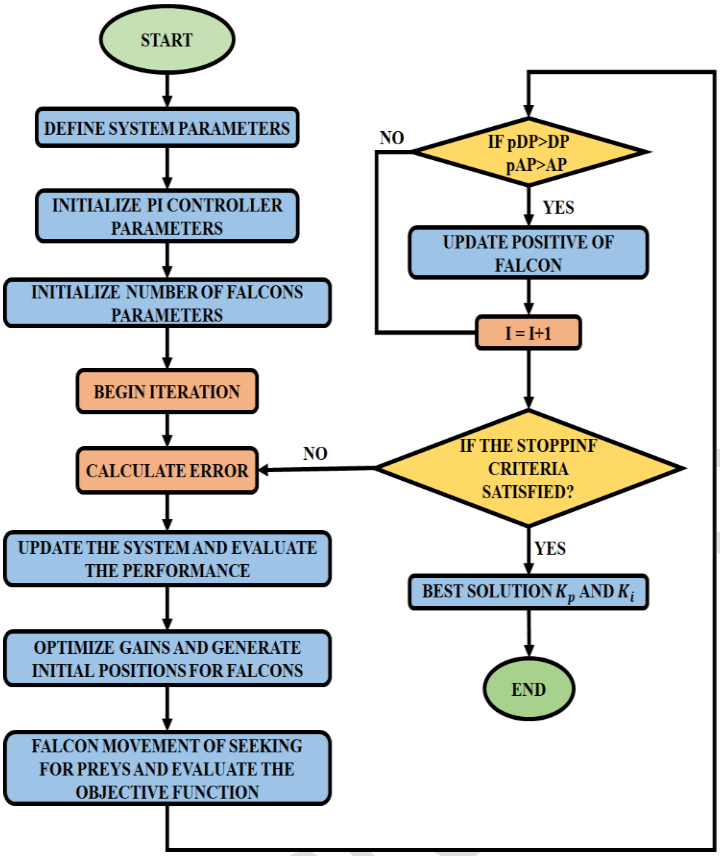

Fig. 7. Flowchart of proposed FOA based PI

The stabilized output with rapid settling time and convergence speed is attained with the aid of proposed optimized controller. On the other hand, in EV battery the bidirectional converter performs essential role for charging and discharging purpose and is explained as below.

2-4- Modelling of Bidirectional DC-DC Converter with Control Approach

The working of BDC converter involves two operations; they are boost and buck operations. If S_1 is held in ON state, S_2 act like a diode. In this case, the BDC converter operates in boost mode. This mode increases the output voltage level. Likewise, if S_2 is ON, then S_1 is work like a diode. The operation in this case called buck operation, and the output voltage is decrease.

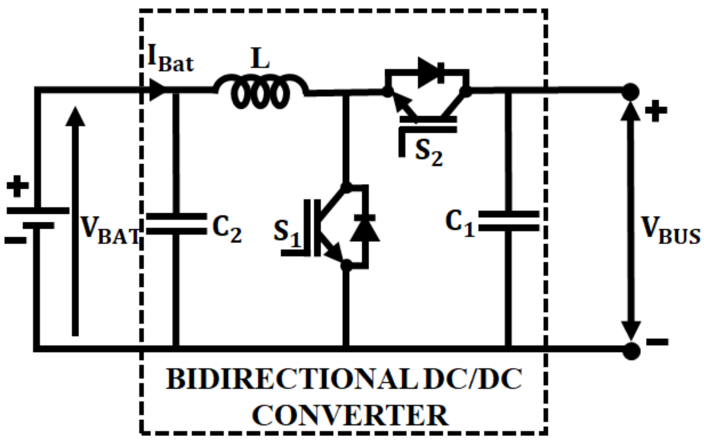

Fig. 8. BDC Converter Circuit Diagram

From the practical applications for EV charging, the EV battery can't be considered as a resistive load due to the nonlinearity of the charging process and dependency on parameters such as SOC, battery voltage, charging current, and the behavior of the converter used. Hence, for this work, the model is consider the EV as a dynamic load of the battery along with a BDC converter. The charging current and battery terminal voltage is controlled using an ANN-based bidirectional converter to simulate EV charging behavior. Battery terminal voltage is stated as:

$$V_{bat} = V_{oc} - I_b R_b \tag{23}$$

Here: V_{bat} : Battery terminal voltage, V_{oc} : Open circuit voltage, I_b and R_b: Battery current, Internal battery resistance. SOC changes of EV battery are computed by:

$$SOC(t) = SOC_0 - \frac{1}{Q}\int i_b(t)\,dt \tag{24}$$

Here: SOC_0: Initial battery SOC, Q : Battery capacity, $i_b(t)$: Battery charging current. Therefore, EV system operates as a controlled nonlinear load, unlike a resistive load, to realistically analyze charging efficiency, voltage control, converter response, and harmonic analysis. The BDC converter's dynamic model is described as, In Boost operation, where S_1 is always ON and S_2 functions as a diode.

$$\begin{bmatrix} \dot{x}_1 \\ \dot{x}_2 \end{bmatrix} = \begin{bmatrix} 0 & -\frac{1}{L} \\ \frac{1}{C_1} & -\frac{1}{R_{load}C_1} \end{bmatrix} \begin{bmatrix} x_1 \\ x_2 \end{bmatrix} + \begin{bmatrix} \frac{x_2}{L} \\ -\frac{x_1}{C_1} \end{bmatrix} u_1 + \begin{bmatrix} \frac{1}{L} \\ 0 \end{bmatrix} x_2 \tag{25}$$

In Buck operation, where S_2 is always ON and S_1 operates as a diode.

$$\begin{bmatrix} \dot{x}_1 \\ \dot{x}_2 \end{bmatrix} = \begin{bmatrix} 0 & -\frac{1}{L} \\ \frac{1}{C_2} & -\frac{1}{R_{bat}C_2} \end{bmatrix} \begin{bmatrix} x_1 \\ x_2 \end{bmatrix} + \begin{bmatrix} \frac{x_2}{L} \\ 0 \end{bmatrix} u_2 \tag{26}$$

Where $x = [i_L V_{bus} V_{bat}]^T$ denotes state vector and i_L stands inductor current, V_{bus} indicates DC link voltage and V_{bat} stands battery voltage. In addition, an ANN controller is employed to optimize converter performance by controlling both the voltage and current levels. The controller takes into account various factors, such as the particular input to the controller. Initially, the difference between computed and actual DC-link voltages is evaluated and then transmitted to ANN controller, which generates phase-shift angle. Finally, the actual voltage is compared with desired voltage, and difference between the two inputs to the ANN controller determines the necessary modulating signal.

ANN Training and Nonlinear Control Characteristics

In the proposed EV charging framework, the association between the control error and the PWM duty cycle is nonlinear because of the dynamic nature of bidirectional converter, EV battery charging behavior, converter switching actions, and fluctuations in PV output conditions. Traditional linear controllers often face performance constraints under such nonlinear conditions, especially during abrupt load changes and charging mode transitions. To address these challenges, an ANN controller is adopted to create an adaptive nonlinear relationship between the control error and PWM signal generation. The ANN controller takes error and change in error as input variables and produces required PWM duty cycle for effective converter regulation. The ANN model is trained offline in MATLAB using a supervised learning approach. Training samples are obtained from converter operation under different loading scenarios, SOC conditions, and PV irradiance variations. The training input parameters include: DC-link voltage error, Change in error, Battery current, SOC level. The corresponding target output is the optimal PWM duty ratio needed to maintain stable converter performance. The Levenberg–Marquardt optimization technique is used to decrease Mean Square Error (MSE) between the estimated PWM output and reference PWM signal. Once the training process converges, the trained ANN weights are transferred into the MATLAB/Simulink platform for real-time controller implementation.

Control action achieved by forming the equations of both boost and buck modes as mentioned below.

$$V_{EVBattery} = V_{DCLink} - L_0 . \frac{dl_{Charging}}{dt} \tag{27}$$

$$I_{Charging} = \frac{1}{L_0} . \int_0^{T_{on}} \left(V_{DCLink} - V_{EVBattery} \right) . dt \tag{28}$$

$$V_{EVBattery} = -L_0 . \frac{dl_{Charging}}{dt} \tag{29}$$

$$I_{Charging} = \int_{T_{on}}^{T_{off}} \left(- \frac{V_{EVBattery}}{L_0} \right) . \mathrm{dt} \tag{30}$$

$$V_{EVBattery} = L_0 . \frac{dl_{Charging}}{dt} \tag{31}$$

$$I_{Charging} = \frac{1}{L_0} \int_0^{T_{on}} \left(V_{EVBattery} \right) . dt \tag{32}$$

$$V_{EVBattery} + V_{L0} = V_{DCLink} \tag{33}$$

$$I_{Charging} = \frac{1}{L_0} . \int_{T_{on}}^{T_{off}} \left(V_{EVBattery} + V_{DCLink} \right) . dt \tag{34}$$

Where, equation (23) to (26) stands buck mode and equation (27) to (30) denotes boost mode. In addition, to achieve the current controlled loop of the buck-boost converter modes using the battery current references where the battery current reference is negative when charging and positive when discharging. Error calculated between actual battery current and battery current reference defines the duty cycle of the ANN controller output. The duty cycle is then used as an input to the PWM generator as depicted in figure 9.

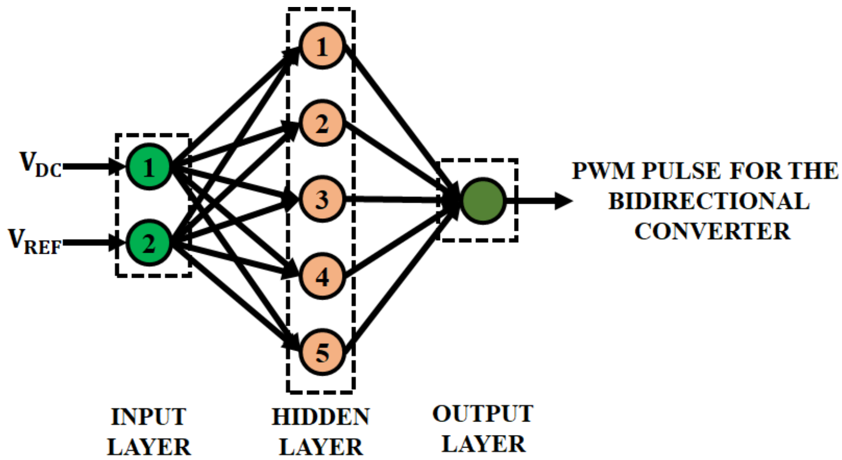

Fig. 9. ANN controller Architecture

By utilizing this system, the converter operation of efficiently regulated, despite this the battery system needs to monitor the SoC with the aid of control technique as dicussed below.

2-5- Modelling of ANN Controller for Battery Charging Level

ANN controller is deployed for monitoring charging and discharging state of EV battery for which it is essential to determine actaul charging level of battery along with SOC. The battery R, V_{oc}, p_{bat} and Q are input parameters that are considered for measuring output voltage on basis of SOC which is illustrated in figure 10. The ANN controller supports estimation and supervision of battery charging state by utilizing battery parameters and SOC dynamics. The SOC estimation of battery is mathematically expressed through the following governing equation, whereas the ANN is applied for adaptive forecasting and monitoring of the charging performance.

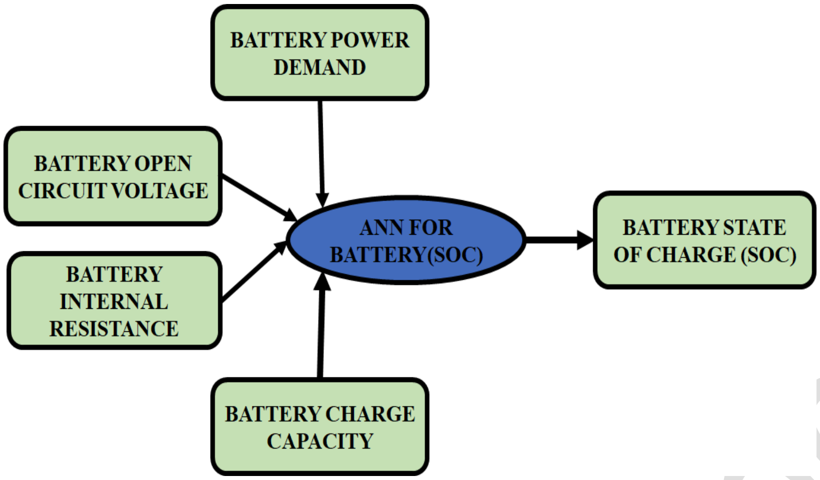

Fig. 10. ANN controller for Battery charging level

$$SOC = \frac{VOC(SOC) - \sqrt{VOC(SOC)2 - 4P\ batteryR}}{2QR} \tag{35}$$

Equation (31) defines mathematical model used for estimating the SOC of EV battery system. The ANN controller does not substitute this equation directly; rather, it is trained to understand the nonlinear charging dynamics and battery characteristics using datasets derived from SOC values, battery voltage, charging current, and operating conditions. Therefore, the ANN functions as an intelligent estimation and monitoring controller to ensure precise supervision of the battery charging process. Moreover, by utilizing the SOC value and proper gear ratio, proper power source is chosen thereby, improving overall efficiency of battery.

3. Results and Discussion

Proposed High Gain Luo converter with Falcon Optimised PI controller is validated by utilizing MATLAB/Simulink outcomes are deliberated in this section. Furthermore, outcomes attaines are compared with other existing converter for the evaluation of efficiency, THD and Voltage gain which are discussed below and the specification for suggested system as depicted in Table 1.

Table 1. Parameter Specification

Parameters	Values

Number of cells connected in series	3
Short circuit current	8.95A
Open circuit voltage	37.25V
Number of cells connected in parallel	7
Modified Luo converter	
L_1, L_2	$4.7mH$
Switching Frequency	$10KHz$
C_1, C_2	$22\mu F$

3-1-Luo converter 1

Contant state

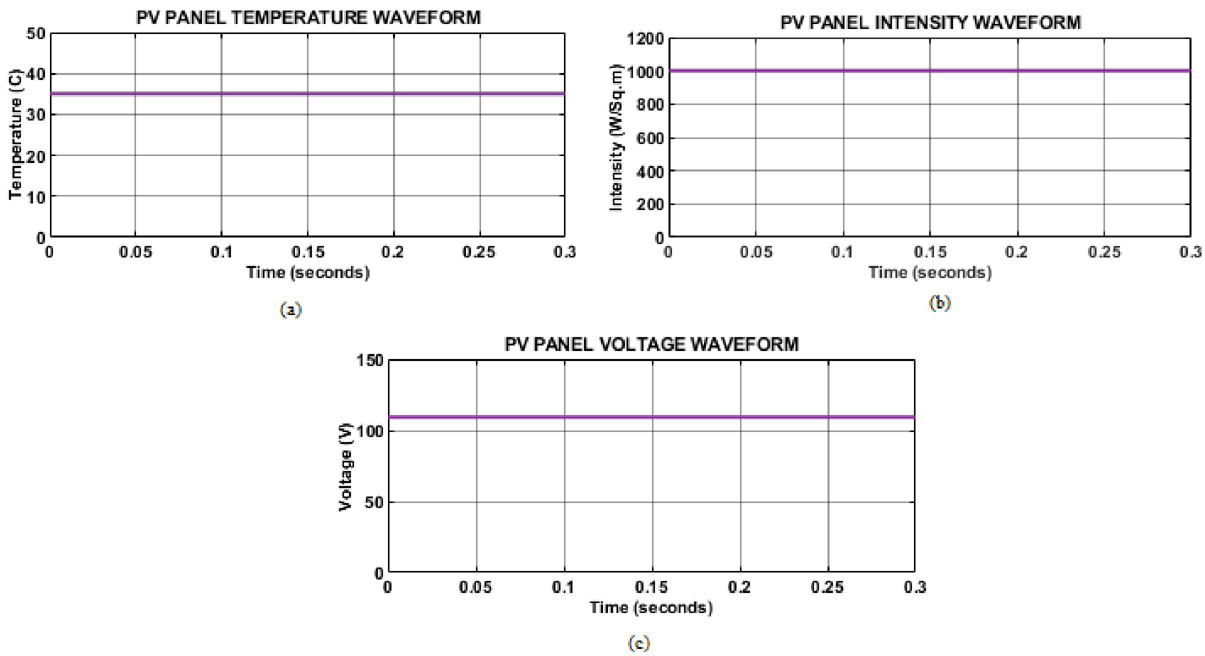

Fig. 11. PV panel waveforms

Figure 11(a) represents PV panel temperature where, temperature remains stable at 35°C during the time period of 0.3 seconds respectively and Figure 11(b) represents PV panel intensity where, intensity stays stable at 1000 W/m² during throughtout the 0.3 seconds respectively. Figure 11(c) represents PV panel voltage which remains constant at 110V throughput 0.3 seconds respectively. Figure 12 represents Luo converter 1 input current which gradually increases to 25.64A after 0.02seconds respectively.

10.22060/EEJ.2026.25018.5819

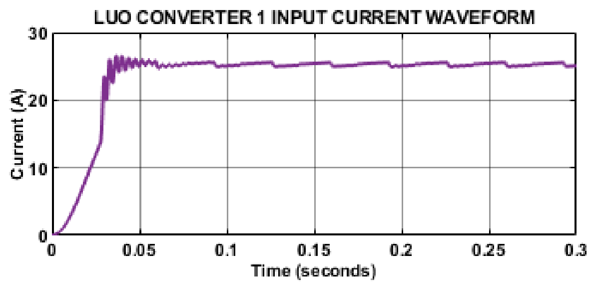

Fig. 12. Waveform of input current for Luo converter 1

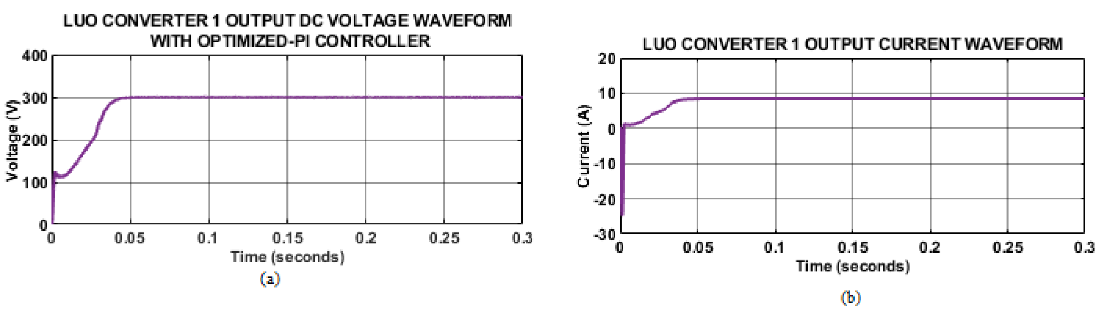

Fig. 13. Waveform of output DC volatage and current for Luo converter 1

Figure 13(a) represents Luo converter 1 with Optimized PI controller's output DC voltage which increases 110V at 0 seconds and further gradually increases to 300V after 0.05 seconds and then stays constant throughout the duration. Figure 13 (b) represents Luo converter 1 Output current which gradually increases to 9 A and then remains stable after 0.05 seconds respectively.

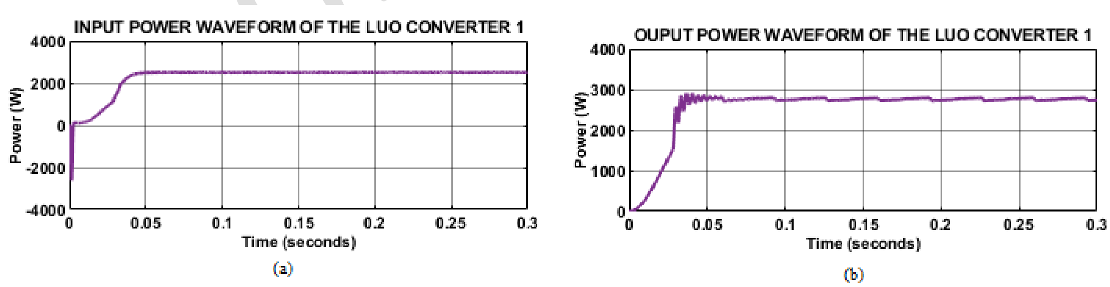

Fig. 14. Waveform of input and output power for Luo converter 1

10.22060/EEJ.2026.25018.5819

Figure 14(a) represents Luo converter 1 input power which gradually increases to attain 2820 W and then remains stable throughout the 0.3 seconds. Figure 14(b)represents Luo converter 1 output power which gradually increases to 2700 W and further deviates slightly throughout 0.3 seconds.

The efficiency of recommended high gain Luo converter will be determined by output power to input power ratio of the converter. This is done through the formula below:

$$\eta = \frac{P_{out}}{P_{in}} \times 100$$

Where, P_{out} : converter output power, P_{in} : input power from the PV source, η = converter efficiency (%). From the simulation values obtained,

$$P_{in} = 2820W, \;\; P_{out} = 2700W$$

$$\eta = \frac{2700}{2820} \times 100 = 95.73\%$$

Figure 15 represents efficiency of Luo converter 1 where the efficiency remains stable at 95.73% with the aid of proposed Modified Luo converter that enhancing the overall system performance.

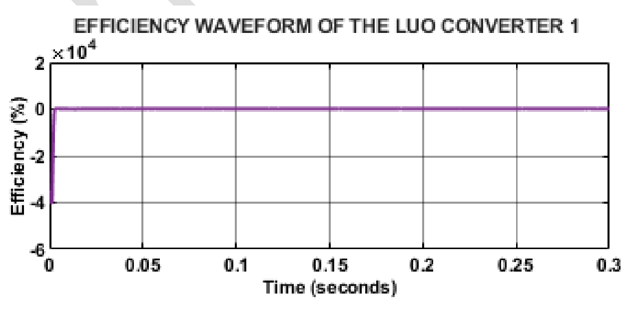

Fig. 15. Luo Converter 1 efficiency waveform

10.22060/EEJ.2026.25018.5819

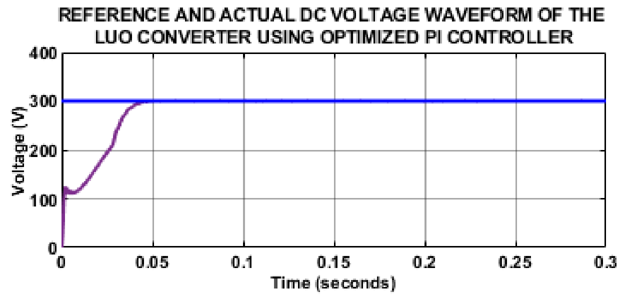

Fig. 16. Waveform of refernce and actual DC voltage of Luo converter using Optimized PI controller

Figure 16 represents waveform of reference and actual DC voltage for Luo converter with optimized PI controller where reference voltage is constant 300V and actual volatge gradually raises to 300 V after 0.04 seconds respectively and Figure 17 represents the waveform of PWM Pulses of the DC-DC converter where the voltage remians within 1V throughout the time duration of 3 seconds respectively.

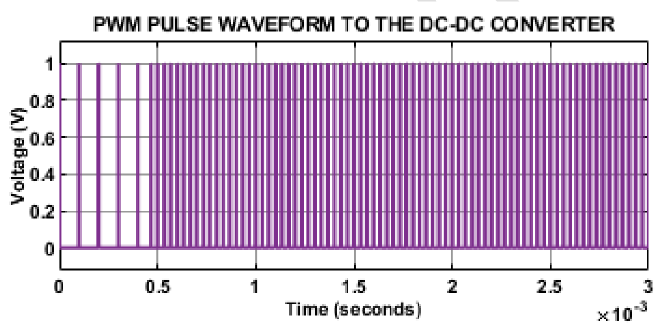

Fig. 17. Waveform of PWM pulses to the DC-DC converter

Varying State

10.22060/EEJ.2026.25018.5819

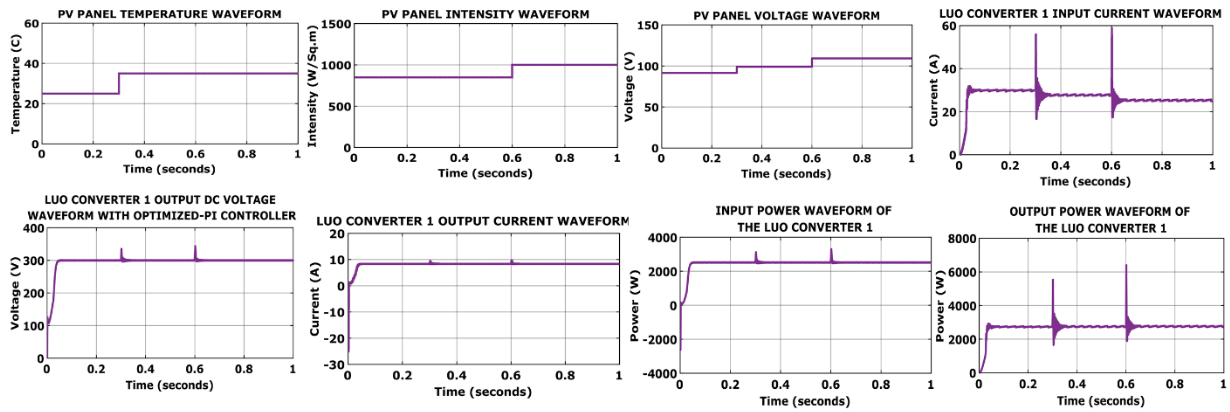

Fig. 18. Varying condition PV and Luo 1 converter waveform in Luo-1 converter

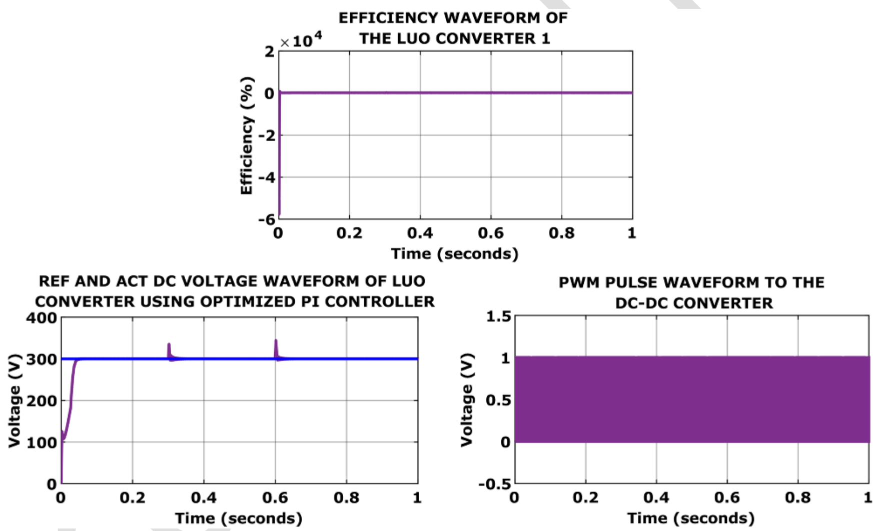

Fig. 19. Luo 1 converter efficiency, Ref and Act voltage, PWM uplse waveform in varying condition

Figure 18(a) shows variation in PV panel temperature under different environmental conditions stays close to 25°Cs. Beyond 0.3 s, the temperature rises to nearly 35°C and remains constant up to the end of the simulation at 1 s. Figure 18(b) presents variation in solar irradiance irradiance is maintained around 800 W/m² and then increases to nearly 1000 W/m². Figure 18(c) illustrates PV panel output voltage under changing irradiance and temperature conditions, voltage initially remains 90 V and gradually increases to 110 V. Figure 18(d) depicts input current waveform of Luo Converter 1. During startup, the converter input

10.22060/EEJ.2026.25018.5819

current quickly increases to nearly 28 A. Due to sudden environmental changes; however, the current rapidly settles near 25.64 A, demonstrating effective controller performance.

An output DC voltage response of Luo Converter 1 controlled by optimized PI controller. The output voltage rises rapidly to 300 V within 0.05 s and maintains a stable regulated value under varying operating conditions, as seen in Figure 18 (e). An output current waveform of Luo Converter 1, initially increases sharply and stabilizes around 9 A, as shown in Figure 18 (f). The input power delivered from the PV source to Luo Converter 1 increases and reaches nearly 2884 W, as depicted in Figure 18 (g). The output power waveform of Luo Converter 1, reaches approximately 2700 W and remains almost constant despite environmental variations, as presented in Figure 18 (h).

Figure 19(a) shows efficiency response of Luo Converter 1, remains nearly constant at 95.73% throughout under different operating conditions. Figure 19 (b) depicts reference and actual DC-link voltage responses of optimized PI controller. The reference voltage is fixed at 300 V, while the actual voltage accurately follows reference within nearly 0.03 s with very small steady-state error and minimal overshoot. Figure 19 (c) presents PWM pulse waveform used for DC-DC converter switching operations within the 0–1 V range and maintains a constant switching frequency throughout the simulation period, ensuring stable converter control and reduced switching-related distortion.

Load condition:

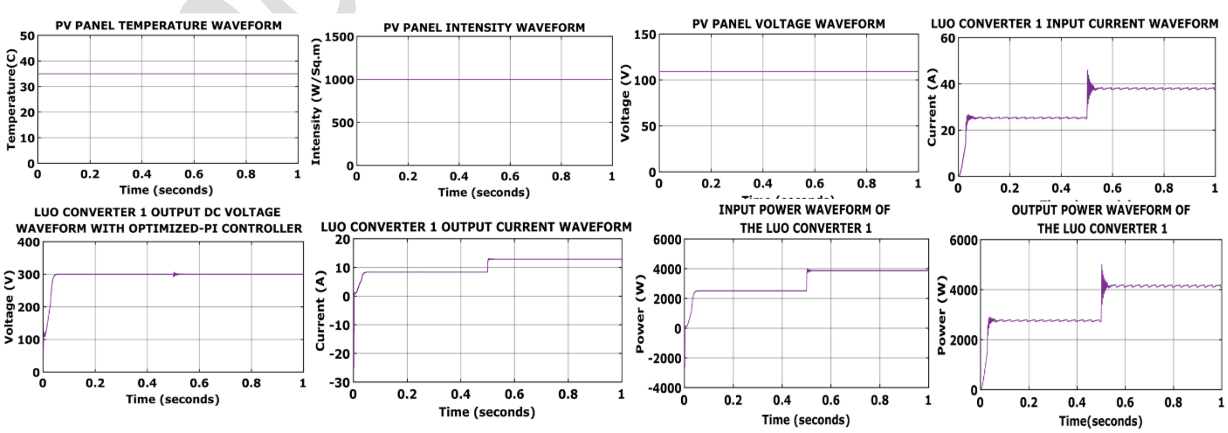

10.22060/EEJ.2026.25018.5819

Fig. 20. Load condition PV and Luo 1 converter waveform

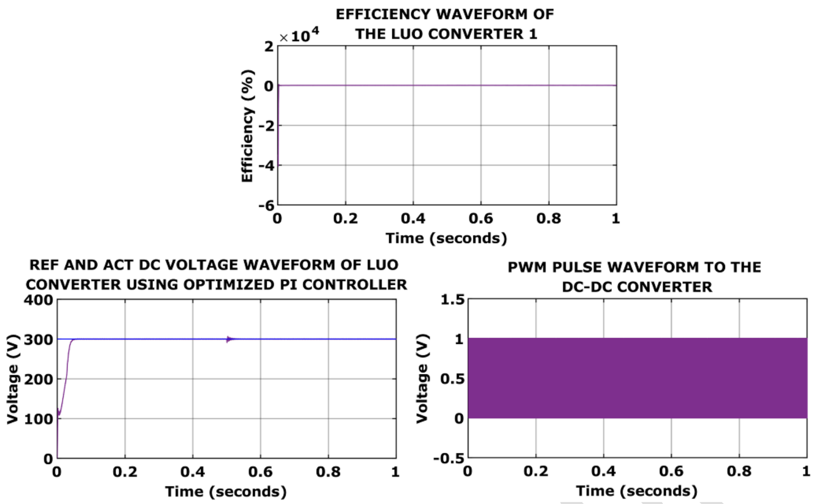

Fig. 21. Luo 1 converter efficiency, Ref and Act voltage, PWM uplse waveform in Load condition

Figure 20(a) presents PV panel temperature waveform under load variation conditions at 35 °C and Figure 20(b) illustrates solar irradiance applied to PV panel maintained at 1000 W/m². Figure 20(c) depicts PV panel output voltage waveform, where the voltage remains stable at 110 V and Figure 20 (d) shows input current waveform of Luo Converter 1 during load variation settles around 25 A. At approximately 0.5 s, the load demand increases, causing the converter input current to rise to nearly 37 A.

An output DC voltage waveform of Luo Converter 1 using optimized PI controller reaches the reference value of 300 V and output current remains close to 8 A and increases to 13 A after 0.5 s due to the increase in load demand, as represented in Figure 20(e) and Figure 20 (f). Theinput power waveform of Luo Converter 1 remains around 2820 W, and after the load variation at 0.5 s, it increases to nearly 4070 W and an output power waveform initially stabilizes near 2700 W and subsequently rises to 3900 W following the load variation, as depicted in Figure 20(g) and Figure 20(h).

Figure 21 (a) illustrates efficiency waveform of Luo Converter 1 under load variation conditions. The converter efficiency remains constant at approximately 95.82% and Figure 21(b) presents reference and actual DC-link voltage waveforms of optimized PI controller is maintained at 300 V, while the actual voltage accurately follows reference with negligible steady-state error and rapid transient recovery during load disturbances. Figure 21 (c) shows PWM pulse waveform generated for DC–DC converter switching operation remains stable within the range of 0–1 V throughout the simulation duration, ensuring reliable switching performance and effective converter control.

3-2- PV Luo Converter 2

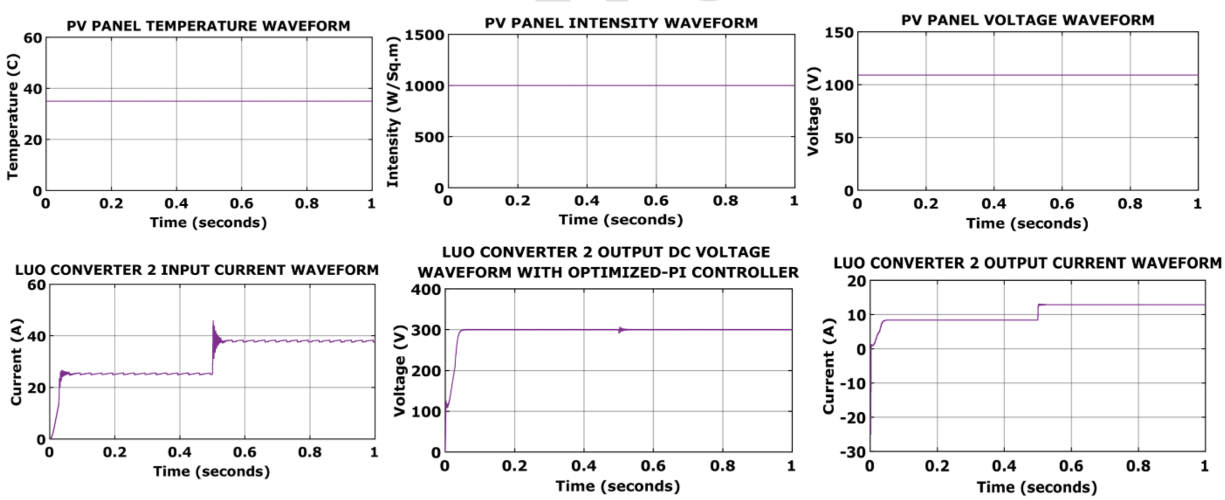

Fig. 22. Waveform of PV panels and Output DC voltage and current fot Luo converter 2

Figure 22 (a) represents the waveform of PV panel temperature which remain stable ar 35° C during the time interval of 0.3 seconds respectively and Figure 22 (b) represents the intensity waveform of PV panel in which, intensity stays stable at 1000 W/m². Figure 22 (c) represents waveform of PV panel Voltage

10.22060/EEJ.2026.25018.5819

where, voltage remains stable at 110 V during the time period of 0.3 seconds respectively. Additionally, Figure 22 (d) represents waveform of luo converter input current which starts to increase gradually to 25.64 A respectively. The DC voltage waveform for Luo converter 2 with Optimized PI controller where the voltage rapidly increases to 110V and further gradually increases to 300V respectively, as seen in Figure 22 (e). The waveform of output current for Luo converter 2 in which the current gradually raises to 9A and then stays stable after 0.05seconds respectively, as revealed in Figure 22 (h).

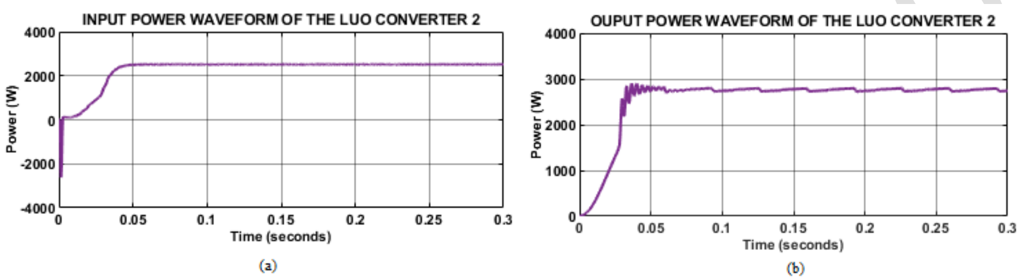

Fig. 23. Input and output power for Luo converter 2

Figure 23 represents the output power waveform in which the power gradually increases to 2700W and maintains throught the 0.3 seconds respectively and the effciency waveform of Luo converter 2 is given in Figure 24 where the efficiecny remains at 95.73% thereby, providing enhanced system performance.

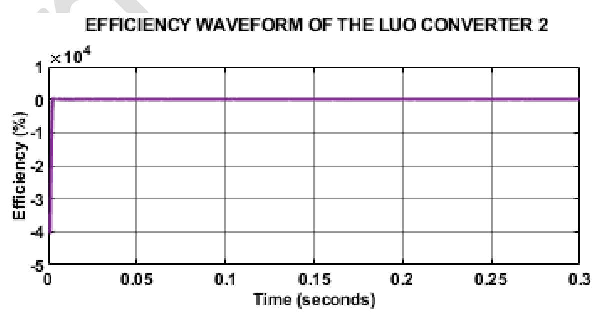

Fig. 24. Waveform of efficiency for Luo converter 2

10.22060/EEJ.2026.25018.5819

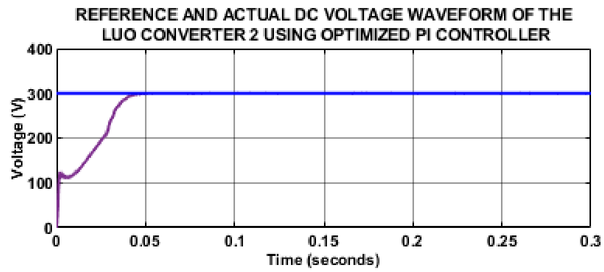

Fig. 25. Waveform of reference and actual DC voltage for Luo converter 2 with Optimized PI controller

Figure 25 represents the reference and actual DC voltage waveform of Luo converter 2 using Optimized PI controller in which the reference voltage stays stable at 300V whereas, the actual voltage gradually raises to 300V respectively and Figure 26 represents DC-DC converter PWM pulse waveform where the voltage stays between 1 V along the time interval of 3 seconds respeectively.

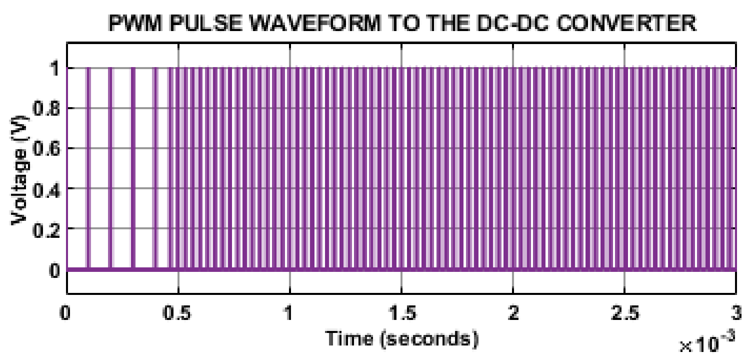

Fig. 26. DC-DC converter PWM Pulse waveform

Varying condition

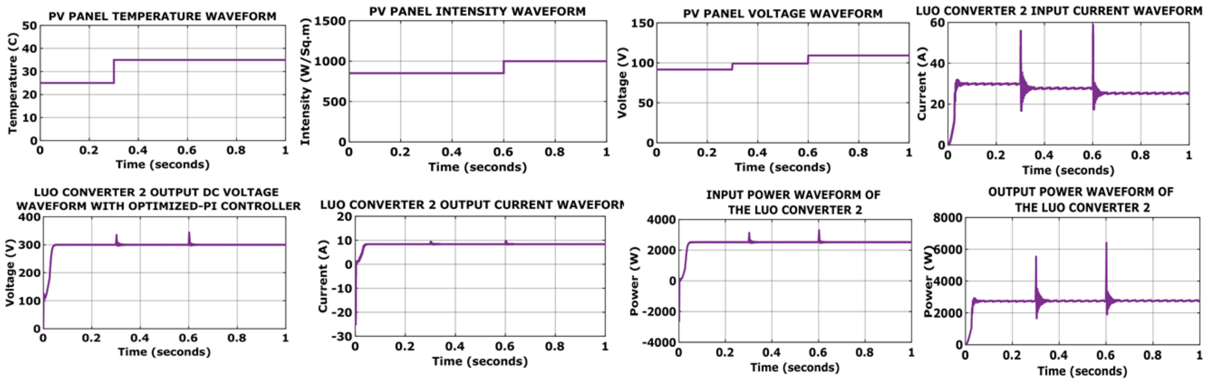

Fig. 27. Varying condition PV and Luo 2 converter waveform

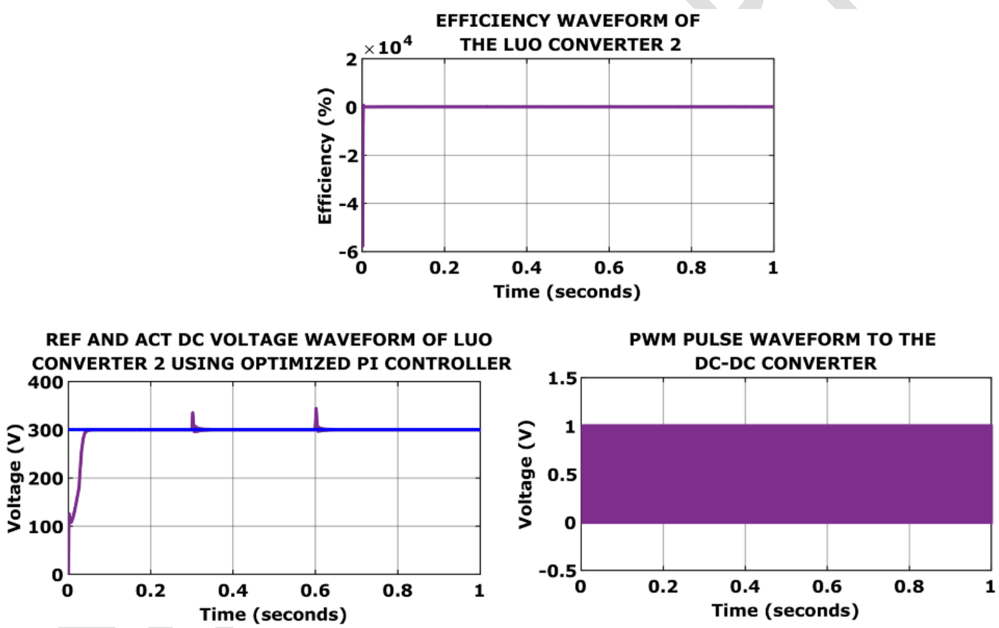

Fig. 28. Luo 2 converter efficiency, Ref and Act voltage, PWM uplse waveform in Varying condition

Figure 27 (a) illustrates PV panel temperature waveform corresponding to Luo Converter 2. Initially, the temperature remains around 25 °C. After 0.3 s, the temperature rises to 35 °C and Figure 27 (b) presents solar irradiance waveform initially remains 800 W/m² and increases to 1000 W/m². Figure 27 (c) depicts PV panel output voltage waveform initially remains 90 V and gradually increases to 110 V and Figure 27

10.22060/EEJ.2026.25018.5819

(d) shows input current waveform of Luo Converter rapidly rises to 28 A however, the current quickly stabilizes near 25.64 A.

An output DC voltage waveform of Luo Converter 2 using the optimized PI controller rapidly reaches 300 V and output current increases and stabilizes around 9 A, as depicted in Figure 27 (e) and Figure 27 (f). An input power waveform rapidly increases and reaches 2820 W and output power waveform increases to nearly 2700 W and remains stable throughout the simulation period, as shown in Figure 27 (g) and Figure 27 (h).

Figure 28 (a) illustrates efficiency constant at 95.72% demonstrating high-efficiency performance of proposed High Gain Luo converter and Figure 28 (b) shows reference and actual DC-link voltage using optimized PI controller is maintained at 300 V, while the actual output voltage accurately tracks the reference value with negligible steady-state error and rapid transient recovery. Figure 28 (c) represents PWM pulse signal remains stable within the range of 0–1 V during the entire simulation interval, ensuring reliable switching operation and enhanced converter control performance.

Load Condition

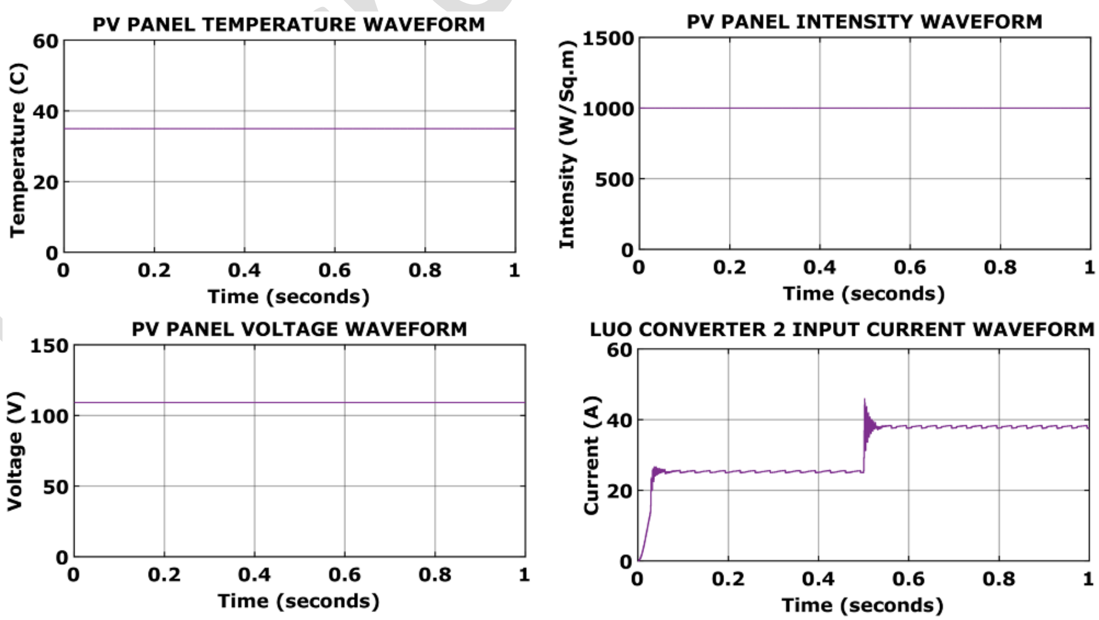

10.22060/EEJ.2026.25018.5819

Fig. 29. Load condition PV waveform in Luo-2 converter

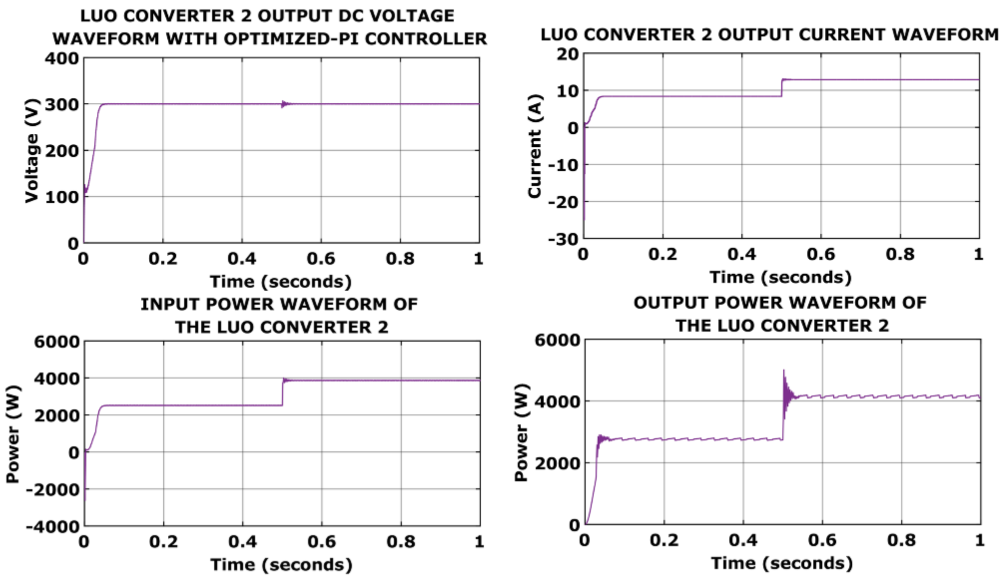

Fig. 30. Load condition of Luo 2 converter power waveform

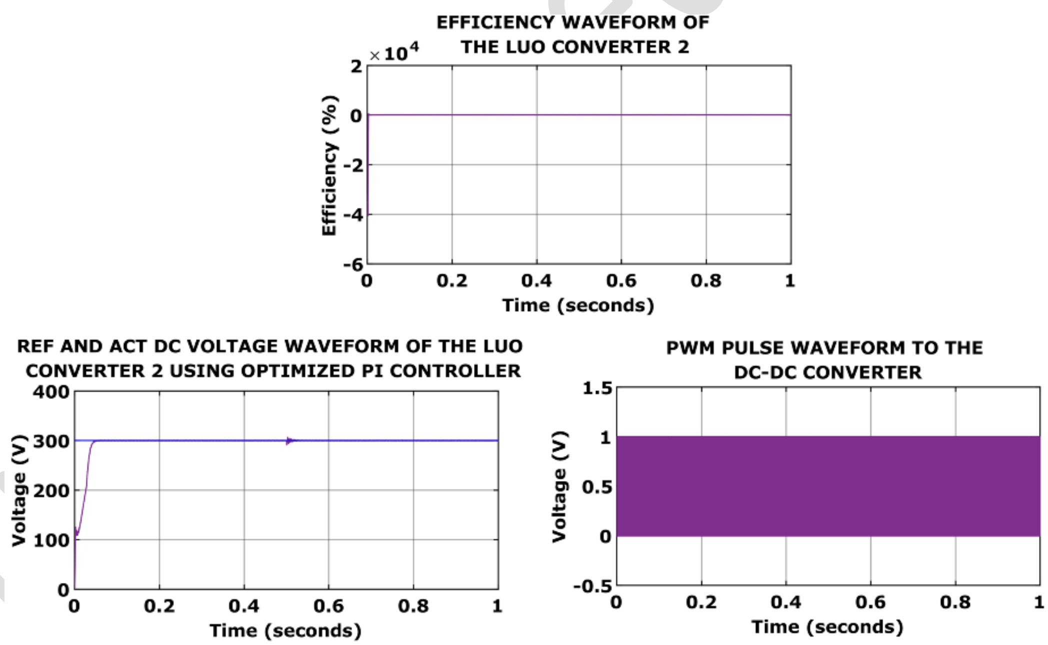

Fig. 31. Luo 2 converter efficiency, Ref and Act voltage, PWM uplse waveform in Load condition

Figure 29 (a) shows PV panel temperature waveform under load variation conditions for Luo Converter 2 constant at 35℃ and Figure 29 (b) represents irradiance waveform for PV panel. The solar irradiance remains almost constant at 1000 W/m², ensuring continuous power production by PV source. Figure 29 (c) represents PV panel output voltage constant at 110V and Figure 29 (d) represents Luo Converter 2 input current is stable at 25A, but after 0.5 seconds when the demand increases, the input current also increases up to 37A.

Figure 30 (a) depicts output DC voltage waveform of Luo Converter 2 under load variation conditions with an optimized PI controller reference level of 300V and Figure 30 (b) shows output current waveform of Luo Converter 2 is almost 8A, but when the load increases after 0.5 seconds, the output current level increases to 13A. Figure 30 (c) shows input power waveform initial value of 2820W; but after load variations, the input power level increases to 4070W and Figure 30 (d) shows output initially stabilizes at a level of 2700W; and then due to load variation, it rises to 3900W.

Figure 31 (a) shows efficiency waveform of Luo Converter 2 remains constant at 95.82% and Figure 31(b) depicts Luo Converter 2 reference voltage is maintained at 300V level, and the actual output voltage level also remains stable with negligible steady-state errors during the entire simulation period. Figure 31 (c) shows PWM pulse waveform supplied from the optimized PI controller for switching operations in the DC-DC converter.

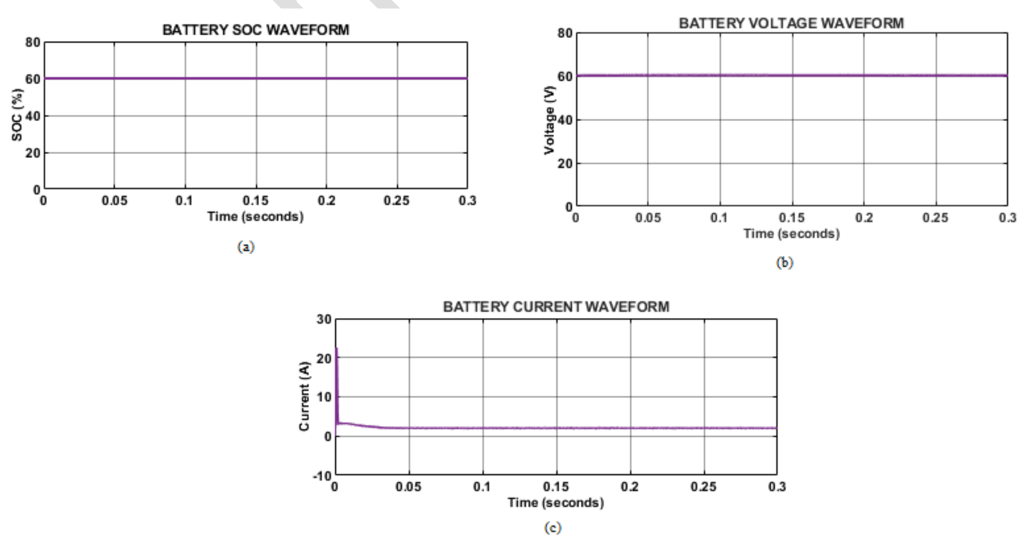

10.22060/EEJ.2026.25018.5819

Fig. 32. Battery Waveforms

Figure 32 (a) represents the waveform of battery SOC which is stable at 60% throughout 0.3 seconds. Battery voltage wavefrom in Figure 32(b) indicates voltage remains constant at 60V throughout 0.3 seconds respectively, where battery current stays constant at 2 A for 0.3 seconds as shown in Figure 32 (c) respectively.

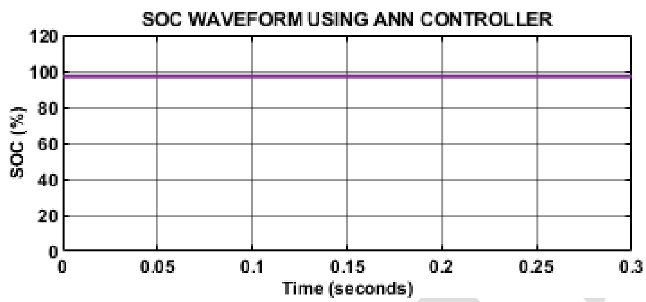

Fig. 33. Waveform of SOC using ANN controller

The SOC waveform using ANN controller in depicted in Figure 33, in which SOC % remains continual at 90% during time interval of 0.3 seconds by monitoring with the aid of ANN controller respectively.

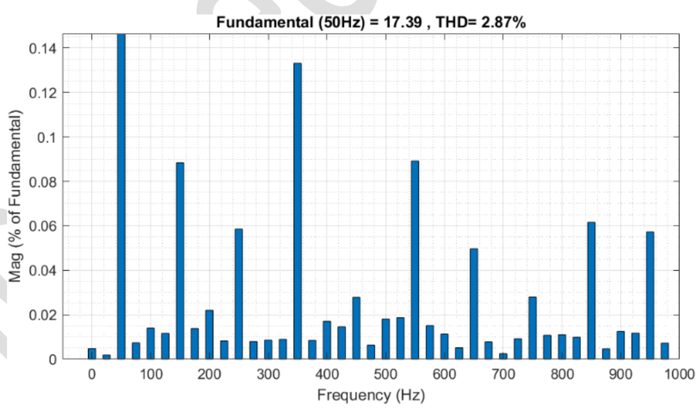

Fig. 34. THD grid current waveform

Figure 34 shows harmonic spectrum along with the THD evaluation of the grid-connected current obtained from proposed dual PV-based EV charging system. The FFT examination is carried out on inverter output current during steady-state operation. The outcomes specify High Gain Luo with FOA-PI controller

10.22060/EEJ.2026.25018.5819

effectively minimizes lower-order harmonics and attains a low THD value of 2.87%, meeting IEEE power quality requirements. The minimized harmonic distortion enhances grid power quality, charging reliability, and overall converter efficiency.

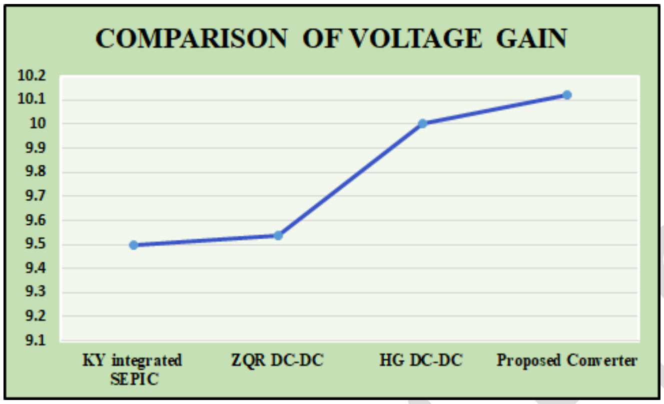

Fig. 35. Voltage gain Comparison

Figure 35 represents Voltage gain comparison of proposed converter with other traditonal converters and from above graph it is notable that proposed converter obtained high voltage gain when compared to other converters, KY integrated SEPIC-9.50 [16] , ZQR DC-DC-9.54 [17] and HG DC-DC -10 [18] respectively.

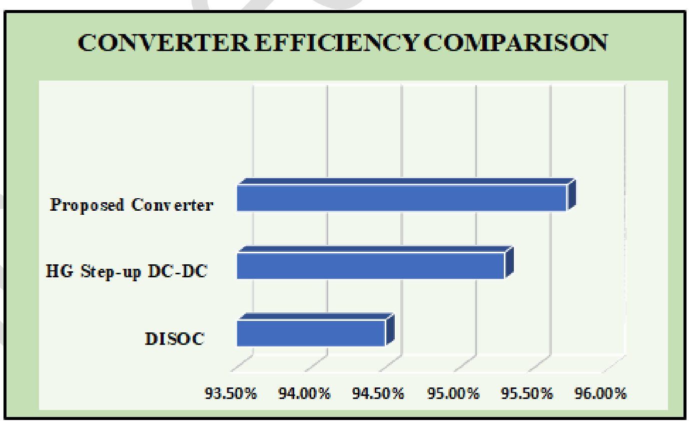

Fig. 36. Efficiecny comparison of converter

Figure 36 represents comparison of efficiency between proposed converter and traditional converters. Proposed converter attained higher efficiency (95.73%) when compared to other traditional converters like DISOC (94.50%) [19] and High Gain Step-up DC-DC converter (95.30%) [20] respectively.

10.22060/EEJ.2026.25018.5819

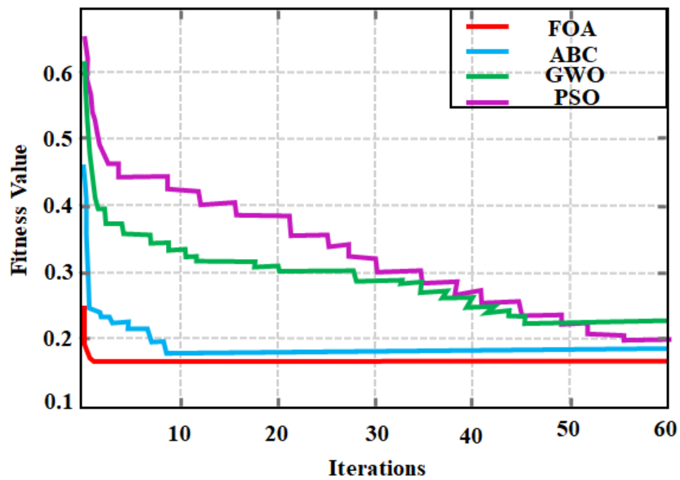

Fig. 37. Comparison of convergence speed

The proposed Falcon optimization appraoch is compared with the recently utilized appraoches such as Artificial Bee Colony (ABC) [21], Gray Wolf Optimization (GWO) [22], Particle Swarm Optimization (PSO) [23] for proving the advantage of utilizing the proposed optimization appraoch as shown in Figure 37,which indicates that the proposed appraoch attains better convergence speed and fitness function, thereby the settling time is efficienly improved compare to the other approaches.

Table 2. Dynamic performance comparison of controllers

Performance Parameter	**Conventional PI**	**FOA-Optimized PI**
Rise Time	0.045s	0.01s
Settling Time	0.08s	0.05s
Peak Overshoot	8.6%	1.5%
K_p	0.8	1.42
K_i	45	68

Table 2 presents a comparison between conventional PI and proposed FOA-PI controller in terms of dynamic performance. FOA-PI controller provides lower rise time and settling time with reduced overshoot and steady-state error because of optimal adjustment of controller parameters. FOA effectively tunes the PI

10.22060/EEJ.2026.25018.5819

gains to obtain faster dynamic response, better voltage regulation, shorter settling duration, and lower harmonic distortion. In addition, the proposed controller enhances harmonic characteristics and improves the overall efficiency of the converter, indicating better steady-state and dynamic performance for EV charging system applications.

4. Conclusion

This papers proposes a Dual PV powered EV charhing system using High Gain Luo converter with FOA-PI controller to attain highly efficienct and sustainable EV charging. The development of this system leads to enhnaced EV charging system utilizing PV power thereby, producing limited carbon emission. The integration of High gain Luo converter assures improved voltage gain, power quality with reduced cost. Significantly, utilizing Falcon Optimised PI controller, produces highly stabilised output with improved convergence speed and reduced settling time. Additionally, Bidirectional converter efficiently charge and discharge state in which current and voltage is controlled by utilizing an ANN controller. In addition to that, ANN controller is proficiently monitored the battery charging level which enables accurate and precise detection of battery charging state thereby, attaining improvised PV powered EV charging system with sustainable and stable power output. Thus, for validating the developed work MATLAB/Simulink is utilized and comparative analysis is performed, proposed system attains higher efficiency (95.73%), improves Voltage gain and decrease THD (2.87%) with rapid convergence speed. Hence, this work attains helpful impact on PV based EV charging system leading to enlarged utilization of EV's.

References

[1] Yao, Haotian, Yue Xiang, Chenghong Gu, and Junyong Liu, "Optimal planning of distribution systems and charging stations considering PV-Grid-EV transactions", 2024 IEEE Transactions on Smart Grid.

[2] Zenhom, Islam A., Mostafa F. Shaaban, and Walid A. Omran. "Grid interactive charging of EVs in PV-powered parking lots considering uncertainties." *IEEE Access* 11 (2023): 111292-111301.

10.22060/EEJ.2026.25018.5819

[3] H. M. Abdullah, A. Gastli, L. Ben-Brahim and S. O. Mohammed, “Planning and Optimizing Electric-Vehicle Charging Infrastructure Through System Dynamics”, 2022 in IEEE Access, vol. 10, pp. 17495-17514.

[4] L. Wang, A. Dubey, A. H. Gebremedhin, A. K. Srivastava and N. Schulz, “MPC-Based Decentralized Voltage Control in Power Distribution Systems With EV and PV Coordination”, 2022 in IEEE Transactions on Smart Grid, vol. 13, no. 4, pp. 2908-2919.

[5] S. S. K. Madahi, A. S. Kamrani and H. Nafisi, “Overarching Sustainable Energy Management of PV Integrated EV Parking Lots in Reconfigurable Microgrids Using Generative Adversarial Networks”, 2022 in IEEE Transactions on Intelligent Transportation Systems, vol. 23, no. 10, pp. 19258-19271.

[6] G. H. Reddy, S. Rani Depuru, S. Gope, B. Veera Narayana, and M. Nayak Bhukya, “Simultaneous Placement of Multiple Rooftop Solar PV Integrated Electric Vehicle Charging Stations for Reliability Benefits”, 2023 IEEE Access, vol. 11, pp. 130788-130801.

[7] H. Kraiem, A. Flah, N. Mohamed, M. Alowaidi, M. Bajaj, S. Mishra, N. Kumar Sharma, and S. K. Sharma, “Increasing electric vehicle autonomy using a photovoltaic system controlled by particle swarm optimization”, 2021 IEEE Access, vol. 9, pp. 72040-72054.

[8] K. Balachander, A. Amudha, M. Siva Ramkumar, G. Emayavaramban, S. Divyapriy, and P. Nagaveni, “Design and analysis of modified CUK converter for electric hybrid vehicle”, 2021 Materials Today: Proceedings, vol. 45, pp. 1691-1695.

[9] Priyadarshi, Neeraj, Pandav Kiran Maroti, and Mohamed G. Hussien. "Extensive performance investigation of Luo converter-based modified firefly maximum point tracking algorithm for permanent magnet synchronous motor-driven photovoltaic pumping system." *IET Renewable Power Generation* 19, no. 1 (2025): e12520.

[10] Karmaker, Ashish Kumar, Md Alamgir Hossain, Hemanshu Roy Pota, Ahmet Onen, and Jaesung Jung. "Energy management system for hybrid renewable energy-based electric vehicle charging station." IEEE Access 11 (2023): 27793-27805.

[11] D. Mazumdar, P. Kumar Biswas, C. Sain, and T. Selim Ustun, “GAO Optimized Sliding Mode based Reconfigurable Step size Pb &O MPPT Controller with Grid Integrated EV Charging Station”, 2023 IEEE Access.

[12] J. A. Glenn, and S. Alavandar, “Hybrid optimized PI controller design for grid tied PV based electric vehicle”, 2023 Intell Autom Soft Comput, vol. 36, no. 2, pp. 1523-1545.

[13] A. AS Mohamed, A. El-Sayed, H. Metwally, and S. I. Selem, “Grid integration of a PV system supporting an EV charging station using Salp Swarm Optimization”, 2020 Solar Energy, vol. 205, pp. 170-182.

[14] Alshareef, Muhannad J. "An effective falcon optimization algorithm based MPPT under partial shaded photovoltaic systems." IEEE access 10 (2022): 131345-131360.

[15] Hassan, Waqas, John Long Soon, Dylan Dah-Chuan Lu, and Weidong Xiao. "A high conversion ratio and high-efficiency bidirectional DC–DC converter with reduced voltage stress." IEEE Transactions on Power Electronics 35, no. 11 (2020): 11827-11842.

[16] G. Vasumathi, V. Jayalakshmi, and K. Sakthivel, “Efficiency analysis of grid tied PV system with KY integrated SEPIC converter,” 2023 Measurement: Sensors, vol. 27, pp. 100767.

[17] S. Harini, N. Chellammal, B. Chokkalingam, and L. Mihet-Popa, “A novel high gain dual input single output Z-quasi resonant (ZQR) DC/DC converter for off-board EV charging”, 2022 IEEE Access, vol. 10, pp. 83350-83367.

[18] J. Ingilala, and I. Vairavasundaram, “Investigation of high gain dc/dc converter for solar pv applications”, 2023 e-Prime-Advances in Electrical Engineering, Electronics and Energy, vol. 5, pp. 100264.

[19] Kumar GG, Sundaramoorthy K. Dual-input nonisolated DC–DC converter with vehicle-to-grid feature. IEEE Journal of Emerging and Selected Topics in Power Electronics 2020; 10(3): 3324-3336.

[20] Wu YE, Wang JW. Novel high-efficiency high step-up DC–DC converter with soft switching and low component voltage stress for photovoltaic system. Processes 2021, 9(7): 1112.

[21] Tefek, Mehmet Fatih. "Artificial bee colony algorithm based on a new local search approach for parameter estimation of photovoltaic systems." Journal of Computational Electronics 20, no. 6 (2021): 2530-2562.

[22] Bettahar, Fares, Sabrina Abdeddaim, Achour Betka, and Charrouf Omar. "A comparative study of PSO, GWO, and HOA Algorithms for Maximum Power Point Tracking in partially shaded Photovoltaic systems." Power Electronics and Drives 9 (2024).

[23] Eltamaly, Ali M. "A novel strategy for optimal PSO control parameters determination for PV energy systems." Sustainability 13, no. 2 (2021): 1008.